Cavity Quantum Electrodynamics Enables *para-* and *ortho-* Selective Electrophilic Bromination of Nitrobenzene

Braden M. Weight,[*,†] Daniel J. Weix,[‡] Zachary J. Tonzetich,[¶] Todd D. Krauss,[*,§,‖] and Pengfei Huo[*,§,‖]

†*Department of Physics and Astronomy, University of Rochester, Rochester, NY 14627, U.S.A.*
‡*Department of Chemistry, University of Wisconsin-Madison, Madison, WI 53706, U.S.A.*
¶*Department of Chemistry, University of Texas at San Antonio, San Antonia, TX 78249, U.S.A.*
§*Department of Chemistry, University of Rochester, Rochester, NY 14627, U.S.A.*
‖*The Institute of Optics, Hajim School of Engineering, University of Rochester, Rochester, NY 14627, U.S.A.*

E-mail: bweight@ur.rochester.edu; todd.krauss@rochester.edu; pengfei.huo@rochester.edu

Abstract

Coupling molecules to a quantized radiation field inside an optical cavity has shown great promise to modify chemical reactivity. In this work, we show that the ground state selectivity of the electrophilic bromination of nitrobenzene can be fundamentally changed by strongly coupling the reaction to the cavity, generating the *ortho-* or *para-* substituted products instead of the *meta* product. Importantly, these are products that are not obtained from the same reaction outside the cavity. A recently developed *ab initio* approach was used to theoretically compute the relative energies of the cationic Wheland intermediates, which indicate the kinetically preferred bromination site for all products. Performing an analysis of the ground state electron density for the Wheland intermediates inside and outside the cavity, we demonstrate how strong coupling induces reorganization of the molecular charge distribution, which in turn leads to different bromination sites directly dependent on the cavity conditions. Overall, the results presented here can be used to understand cavity-induced changes to ground state chemical reactivity, from a mechanistic perspective, as well as to directly connect frontier theoretical simulation to state-of-the-art, but realistic, experimental cavity conditions.

Introduction

Coupling molecules to a quantized radiation field inside an optical cavity creates a set of photon-matter hybrid states, called polaritons. These polariton states have a great promise to change chemical reactivity in a general and facile way by tuning the properties of matter as well as properties of photons. Despite the theoretical predictions of using polaritons for novel chemistry broadly,[1] experimentally what has been demonstrated largely relates to polariton modified reaction kinetics. For example, collective couplings between the electronic excited states of fulgide or similar molecules and quantized photonic modes inside an optical cavity were shown to both enhance or suppress photochemical isomerization reactions.[2,3] In another example, vibrational excitations collectively coupled to the photonic excitations of a microcavity, commonly referred to as vibrational strong coupling (VSC), resulted in chemical kinetics that can be enhanced[4,5] or suppressed.[6–8] In these two collective coupling regimes, the kinetics of the reactions are changed, but importantly there is no new type of product generated compared to the same reactions outside the cavity.

Recent theoretical investigations[1,9] have suggested that the *ground state* of a molecular system can be significantly modified by coupling the electronic states of a molecule to a cavity photon mode..[10–19] In particular, it has been shown that the cavity can modify the endo/exo selectivity of Diels-Alder reactions,[20,21] modify the ground

state proton transfer reactions barriers and driving forces,[15,16] and selectively control the product of a click reaction.[22] Note that the cavity frequency in these studies is chosen to be in the range of electronic excitations in molecules (in terms of energy, on the order of eV), and thus the resulting polaritonic effects are expected to be different than the more commonly explored VSC regime.[6,8] In addition, for this case cavity-modified chemistry does not require the usual resonance effects of light-matter interactions (*i.e.*, frequency matching between light and matter excitations), since the cavity can directly modify the ground state of the hybrid system, referred to as quantum vacuum fluctuation modified chemistry.[15,20] Importantly, predictions based on single molecules coupled to a cavity are also within the reach of the magnitude of strong coupling shown in recent experiments using a plasmonic nano-cavity.[23] A conceptually understand these recently proposed ground state modifications due to the cavity vacuum fluctuations[9,15,17,20,24–26] are provided in the **Theoretical Methods** section.

The molecule-cavity hybrid system can be described by the Hamiltonian[1,9,27] in Eq. 2. The light-matter coupling strength is expressed as

$$A_0 = \sqrt{\frac{1}{2\omega_c \varepsilon \mathcal{V}}}, \tag{1}$$

where $\mathcal{V}$ is the effective mode volume of the cavity, ε is the permittivity inside the cavity, and ω_c is the cavity frequency. Through the light-matter interactions, various photon-dressed electronic states will be coupled to each other. For example, the ground electronic state with 1 photon in the cavity and an excited electronic state with 0 photons in the cavity will couple through the light-matter interaction. When the energy of these two basis states become close, they interact (mathematically similar to the interaction of atomic orbitals to form molecular orbitals), leading to the formation of excited polariton states. These (and all similar) interactions represent the result of resonant, strong light-matter coupling, causing the formation of new eigenstates, *i,e,* polaritons.

Through non-resonant light-matter interactions, the cavity can directly modify the ground state of a molecule coupled to the cavity. In order to understand this effect, which is important for understanding how cavities can modify ground state chemical reactivity, one has to go beyond the pre-
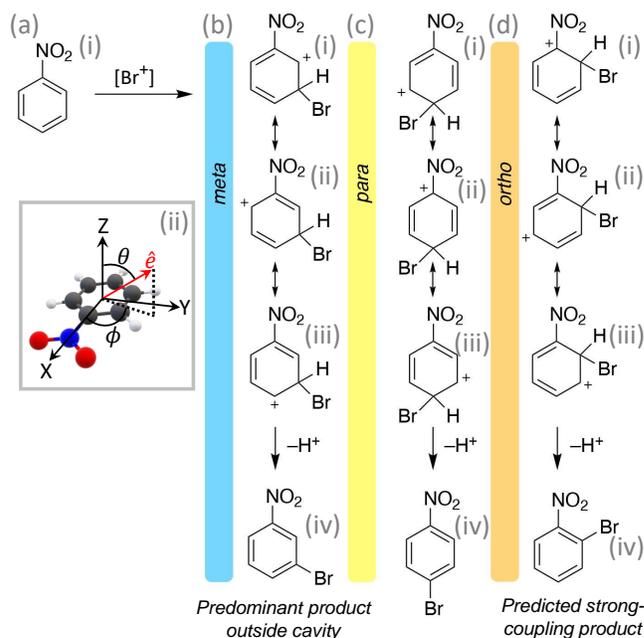
Scheme 1: Bromination reaction of nitrobenzene molecule generally leads to the *meta*-substituted nitrobenzene. The reaction occurs through a well-known cationic intermediate. Coupling this reaction to the cavity allows selective bromination of the *para* (orange) or the *ortho* (red) site of the benzene ring and leads to *para*- and *ortho*-substituted products.

dictions of the simple Jaynes-Cummings model for light-matter interactions.[28] Direct modification of polariton ground states can be caused by two physical processes:[1,9,29] (i) off-resonance light-matter interactions (third term in Eq. 2) through the ground state permanent dipole and optical transition dipoles between the ground and excited states, and (ii) a dipole self-energy term. The detailed theoretical arguments are provided in the **Theoretical Methods** section below Eq. 2.

In this work, we demonstrate that the strong coupling between molecule and cavity can dramatically change the reaction outcome of the bromination of nitrobenzene in its ground state. The bromination of nitrobenzene is a textbook electrophilic aromatic substitution (EAS) reaction,[30,31] where, *meta*-bromination is the predominant product under many standard conditions.[32–37] The observation of exclusively *meta*-bromination has been well-explained by the relative stability of the three possible cationic intermediates of PhNO$_2$-Br$^+$ (see Scheme 1) using resonance structure analysis.[31,38,39] These and similar reactions have also been explored with density functional theory; although in some cases alternative mechanisms have been proposed,[40–44] the

Wheland intermediate explains the regiochemistry for nitrobenzene bromination in polar solvents well.

We apply a recently developed *ab initio* polariton chemistry approach,[16] and theoretically demonstrate that coupling nitrobenzene to an optical cavity can fundamentally change the selectivity of the electrophilic bromination reaction of nitrobenzene, making possible the *ortho-* or *para-*substituted products. We have further provided an analysis of how coupling to the cavity will change the charge distribution of the cationic intermediate, which therefore causes a modification to the preferred bromination site. As such, strong couplings between molecules inside the cavity offer a promising tool[14] to fundamentally change the outcome of a known chemical reactions.

Results and Discussion.

Scheme 1 presents the classic reaction mechanism of the electrophilic bromination of nitrobenzene, which first proceeds through a cationic intermediate (the so-called Wheland intermediate) $PhNO_2$-Br^+, that undergoes subsequent deprotonation to afford the product. In this work, we focus on the cavity modification of the energies of these positively charged reaction intermediates $PhNO_2$-Br^+. This molecule is accepted as the quasi-stable intermediate species in the kinetics of the bromination of nitrobenzene, and the site selectivity of halogenations of aryl species is largely dictated by this intermediate.[30,38,39,45] However, recent experimental and theoretical explorations have demonstrated that other pathways, such as an addition-elimination route, maybe more favored under certain conditions.[40,46,47]

Outside the cavity, the *meta*-intermediate is the most stable for nitrobenzene and provides nearly 100% selectivity due to a favorable set of possible resonance structures. On the other hand, the *para*- and *ortho*-substituted products are not observed due to the presence of high-energy resonance structures. In the case of bromination outside of the cavity, which corresponds to the $A_0 = 0.0$ a.u. and $\omega_c = 0.0$ eV case in Eq. 2, the *meta*-substituted intermediate species is more thermodynamically stable compared to the *ortho-* and *para*-species by roughly 2 and 5 kcal/mol, respectively, confirming this classic reaction mechanism.

Coupling this intermediate with the optical cavity, we find that the energy of the *ortho-* and *para*-substituted intermediate can have lower energy than the *meta*-substituted species under a range of coupling strengths A_0 and cavity frequencies ω_c. The relative energies of different intermediates depend on the orientation of the intermediate relative to the electric field of the cavity. A more stable *ortho*-substituted intermediate is formed if the cavity polarization is along one direction of the molecule (blue regions Fig. 1a, cartesian directions defined in Scheme 1a(ii)) while the *para* substituent becomes stabilized for a different polarization direction (blue regions in Fig. 1b).

To observe a significant change in the polaritonic ground state (due to the non-resonant light-matter coupling terms in the Hamiltonian), it generally requires a very strong light-matter interaction strength between a single molecule and the cavity mode.[9,15,20] This light-matter coupling regime can be realized by using state-of-the-art plasmonic nano-cavities, which provide realistic experimental parameters that were used for these simulations. In these systems,[48,49] the cavity mode volume is extremely small, on the order of $\mathring{A}^3$. For example, a recent nano-cavity achieved a mode volume[50] of $\mathcal{V} = 0.15$ nm³. The coupling strength typically required[20] to observe any interesting changes to the ground state is $\lambda = \sqrt{1/\varepsilon\mathcal{V}} \approx 0.1$ a.u. corresponding to $A_0 \approx 0.3$ a.u. or field strength $\mathcal{E} = 10.8$ V/nm that can be experimentally accomplished[23] Experimentally, the NanoParticle on Mirror (NPoM) cavity structure[51] can achieve such coupling strengths with electric field intensities $\mathcal{E} = \omega_c A_0 \approx 2-10$ V/nm. For the specific case of a gold plasmonic nano-cavity,[48,49] the cavity frequency is $\omega_c = 1.8$ eV. These coupling strengths from NPoM cavities are also consistent with a mode volume of $\mathcal{V} = 0.15$ nm³.

Fig. 1a presents the relative energetic stability of the *meta-* and *ortho*-cationic intermediate species, computed as $E_0^{ortho}(\mathbf{R}) - E_0^{meta}(\mathbf{R})$ inside the cavity, as a function of θ and ϕ. Fig. 1b presents the results of $E_0^{para}(\mathbf{R}) - E_0^{meta}(\mathbf{R})$. The cavity polarization direction $\hat{\mathbf{e}}$ with respect to the $\mathbf{X}$, $\mathbf{Y}$, and $\mathbf{Z}$ directions of the molecule is defined by the polar angle θ and the azimuthal angle ϕ (see Scheme 1a(ii) and the inset of Fig. 1b). In Fig. 1 all possible spatial orientations of the cavity polarization direction $\hat{\mathbf{e}}$ with respect to the molecule are presented. When $\theta = 90°$ and $\phi = 0°$ (or equivalently $\phi = 360°$), $\hat{\mathbf{e}} = \hat{X}$ and when $\theta = 90°$ and $\phi = 90°$, $\hat{\mathbf{e}} = \hat{Y}$.

From Fig. 1, we can see the regions (blue) of θ and ϕ where *ortho-* or *para*-substituted intermediates are more stable than the *meta*-substituted
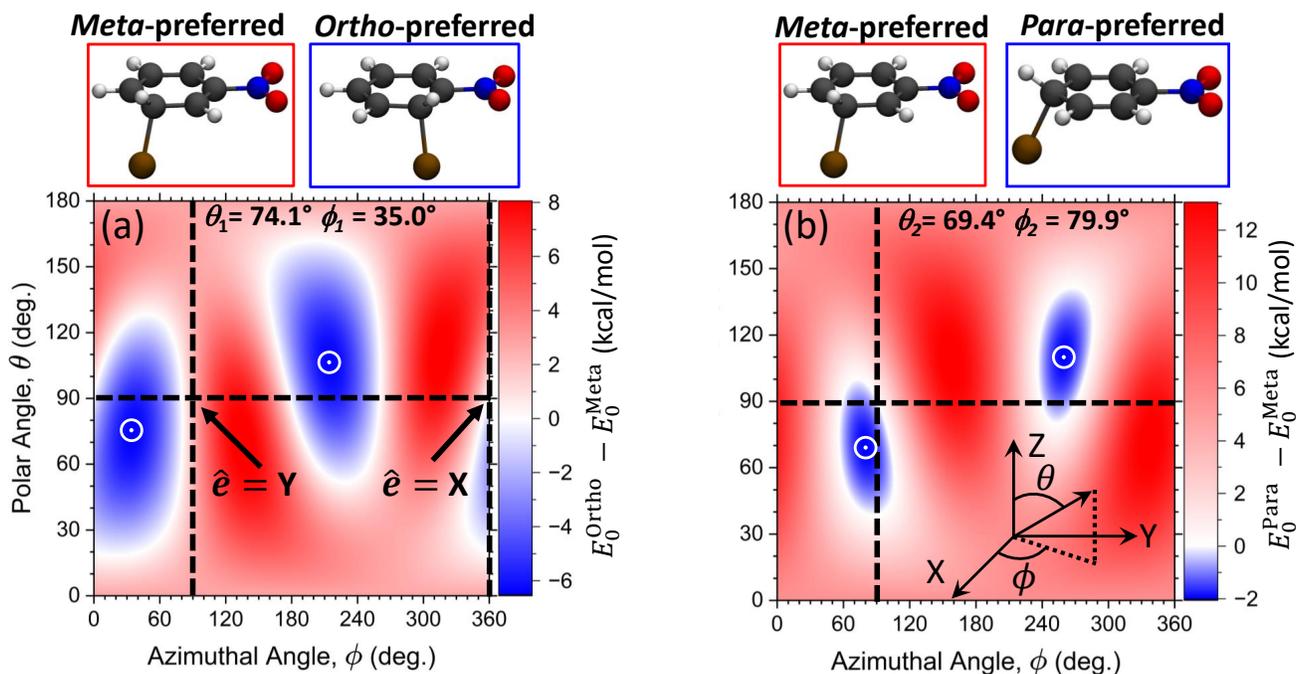
Figure 1: Relative energy of the polaritonic ground states between (a) *ortho*-PhNO$_2$-Br$^+$ and *meta*-PhNO$_2$-Br$^+$ and (b) *para*-PhNO$_2$-Br$^+$ and *meta*-PhNO$_2$-Br$^+$, as a function of the azimuthal $\phi \in [0, 2\pi)$ and polar $\theta \in [0, \pi)$ angles of the cavity polarization vector with respect to the molecular cartesian axes in the inset of panel (b) of this figure. The cavity frequency and coupling strength are fixed at $\omega_c = 1.8$ eV and $A_0 = 0.3$ a.u. (corresponding to a cavity volume of $\mathcal{V} = 0.15$ nm^3 or a field strength of $\mathcal{E} = 10.8$ V/nm). The minimum values of the relative energies in each case are (a) -6.43 kcal/mol and (b) -1.97 kcal/mol, which are denoted by the white open circles.

isomer. For example, the most stable energy for the *ortho*-substituted complex is achieved when $\theta \approx 75°$ and $\phi \approx 35°$, which is 6.4 kcal/mol lower in energy than the *meta*-substituted complex. The most stable energy for the *para*-substituted complex is achieved when $\theta \approx 70°$ and $\phi \approx 80°$, which is 2.0 kcal/mol more stable compared to *meta*-substituted complex. When $\theta = 0°$ for $\hat{\mathbf{e}} = \mathbf{Z}$ or $\theta = 180°$ for $\hat{\mathbf{e}} = -\mathbf{Z}$, the cavity polarization is along $\mathbf{Z}$-direction, where the molecular dipole is nearly zero and the cavity modification diminishes, as expected. Room temperature thermal energy is $k_BT \approx 0.58$ kcal/mol, and for the case of bromination outside the cavity, the *meta*-substituted intermediate species is thermodynamically stable compared to the *ortho*- and *para*-species by roughly 2 and 5 kcal/mol, respectively (see Fig. 4). Thus, these results suggest that by coupling the nitrobenzene molecule to an optical cavity, the preferred bromination sites can be tuned to either *ortho*-substituted or *para*-substituted, whereas outside the cavity, *meta*-substituted products dominate under standard conditions.[30,31] As such, coupling to the cavity allows obtaining the "impossible

products" (*para*- and *ortho*-substituted PhNO$_2$-Br) outside the cavity.

For the single molecule strong coupling case, one often has to control the molecular orientation with respect to the cavity field polarization direction in order to see polaritonic effects on chemistry. For example, recent theoretical work suggests that only when coupling to the cavity along particular electric field directions, one can selectively obtain the endo- or the exo-products of a Diels-Alder reaction,[20] whereas an isotropic random orientation of the molecule will likely end up giving an equal mixture of both isomers, a situation similar to that obtained outside the cavity. Experimentally, it has been shown for a single molecule-NPoM cavity system that controlling the molecular orientation to align the molecule with the cavity field is possible.[48] Nevertheless, perfectly controlling the molecular orientation in all cases is exceptionally challenging.

The currently proposed bromination reaction, on the other hand, does not require precise control of the orientation of molecules, if the goal is to obtain non-*meta*-substituted products in order to demon-
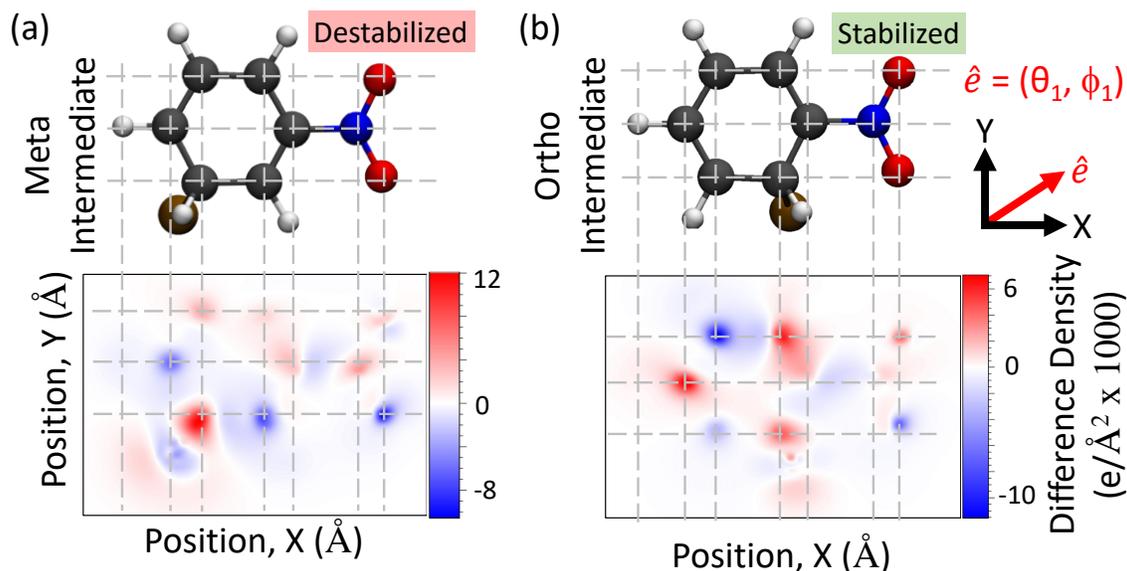
Figure 2: Ground state density difference $\Delta\rho_{00}(x,y) = \int dz[\rho_{00}^{\mathrm{M}}(x,y,z) - \xi_{00}(x,y,z)]$ of (a) the *meta*-cationic intermediate and the *ortho*-cationic intermediate with a light-matter coupling strength $A_0 = 0.3$ a.u. and cavity frequency $\omega_{\mathrm{c}} = 1.8$ eV. The cavity polarization is along $\hat{e} = (\theta_1, \phi_1)$ defined in Fig. 1 with inset to panel (b) showing the projection of the polarization onto the XY-plane. The color bar indicates the magnitude and sign of the difference density $\Delta\rho_{00}(x,y)$, where positive (red) indicates electron charge accumulation and negative (blue) indicates electron charge depletion upon coupling the molecule with the cavity.

strate the use of a cavity to enable novel bromination selectivity under standard reaction conditions. As such, randomly oriented molecules strongly coupled to the nano-cavity will bias the selectivity to favor *ortho-* and *para*-substituted nitrobenzene products. On the other hand, if the objective is to only obtain either *ortho-* or *para*-substituted pure species, then one would either need to control molecular orientation along the cavity field polarization, or separate the mixture of products post-reaction, as is common for bromination of activated arenes.

To further understand the role of the optical cavity in inducing these chemical changes, we compute the ground state electron density difference between molecules placed inside the cavity and outside the cavity. This comparison allows a direct visualization of the cavity-mediated changes to the electron density and facilitates chemical insights into the relative stability of the various substituted reaction intermediates. The difference density function of the ground state is defined as $\Delta\rho(X,Y,Z) = \rho_{00}^{\mathrm{M}}(X,Y,Z) - \xi_{00}(X,Y,Z)$, where ρ_{00}^{M} is the polaritonic ground state electronic density (with the photonic degrees of freedom integrated out) and ξ_{00} is the bare electronic ground state density. Theoretical details for computing

$\rho_{00}^{\mathrm{M}}(X,Y,Z)$ and $\xi_{00}(X,Y,Z)$ are provided in the **Supporting Information**. Further, a discussion regarding the contributions to the polaritonic ground state density matrix with respect to the calculated the electronic densities can be found in the **Supporting Information**. To help visualize the density difference, we further integrate out the Z-direction (perpendicular to the plane of the benzene ring) and present the two-dimensional density differences, $\Delta\rho(X,Y) = \int dZ \Delta\rho(X,Y,Z)$.

Fig. 2 shows the electron density difference when the cavity polarization is along $\hat{\mathbf{e}} = (\theta_1, \phi_1)$ (see Fig. 1a and inset to Fig. 2b for the polarization direction projected onto the XY-plane). The rest of the parameters are the same as in Fig. 1, with $A_0 = 0.3$ a.u. and $\omega_{\mathrm{c}} = 1.8$ eV. Under these conditions, the *ortho*-substituted Wheland intermediate becomes more stable than the *meta*-substituted intermediate (see Fig. 1a) by $\sim$ 6.4 kcal/mol. Fig. 2a shows the density difference for the *meta*-substituted reaction intermediate while Fig. 2b presents the density difference for the *ortho*-substituted reaction intermediate. The color scheme of this plot is: red (positive values) indicates the accumulation of electron density and blue (negative values) indicates depletion of electron density upon coupling of the molecule into

5

the cavity. Fig. S3 in the **Supporting Information** shows data for the *meta* (Fig. S3a) and *para*-substituted (Fig. S3b) intermediate species.

Fig. 2 presents the electron density difference contour maps for the *meta*-substituted and the *ortho*-substituted intermediate species, depicting the cavity-induced localization of the electron density accumulation (red) and depletion (blue). For the *meta*-substituted intermediate species, the bromine-connected carbon accumulates a large amount of electron density when coupling to the cavity, while the adjacent carbons (*ortho* and *para* carbons relative to the nitro group) exhibit strong electron density depletion. On the other hand, the *ortho* intermediate species in Fig. 2b shows a delocalized electron density accumulation on the bromine-connected carbon and the two carbons in the *meta* position relative to the bromine-connected carbon. However, the electron density becomes depleted only at the *para* carbon relative to the bromine-connected carbon (*i.e.*, the carbon opposite the bromine-connected carbon). This reorganization of the electron density allows for the cavity-mediated selectivity of the three cationic intermediate species. In fact, for the *ortho* intermediate species, one can make a direct connection to a resonance structure for the Wheland intermediate which contains a partial positive charge on the carbon opposite the bromine-connected carbon. Thus, the cavity is stabilizing the *ortho* Wheland intermediate by shifting the electronic density to a stable resonance structure depicted in scheme. 1d(ii), in contrast to the destabilizing resonance structure which occurs outside the cavity with a partial positive charge in the nitrogen-connected carbon depicted in Fig. 1d(i).

Fig. 3a presents the relative energetics of the *ortho*- and *meta*-substituted intermediate $E_0^{ortho}(\mathbf{R}) - E_0^{meta}(\mathbf{R})$ when the cavity polarization $\hat{\mathbf{e}} = (\theta_1, \phi_1)$ (see Fig. 1a) as a function of cavity frequency ω_c and the cavity mode volume $\mathcal{V}$ (in units of nm^3). Fig. 3b presents the relative energetics of the *para*- and *meta*-substituted intermediate $E_0^{para}(\mathbf{R}) - E_0^{meta}(\mathbf{R})$ when $\hat{\mathbf{e}} = (\theta_2, \phi_2)$ (see Fig. 1b). Here, we focus on the range of frequency $\omega_c \approx 1 - 4$ eV which is within the typical range possible of nano-cavity designs. The cavity frequency of the NPoM cavity depends on the materials of the nanoparticle, the size of the nanoparticle, and the gap size between the particle and the mirror surface. The typical value is for gold nano-particle about $\omega_c \approx 2$ eV (600 nm), silver
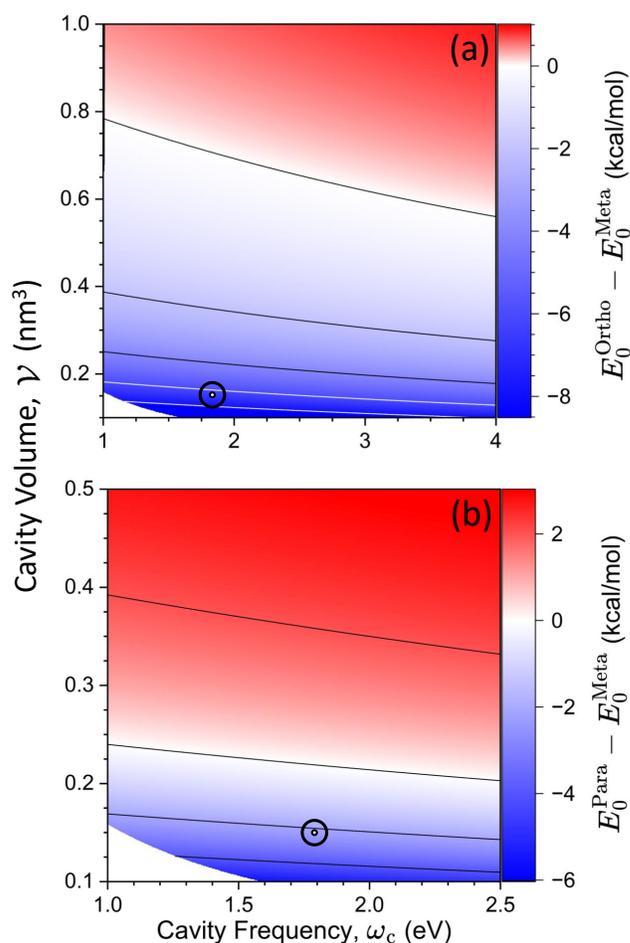
Figure 3: (a) Relative energy of the polaritonic ground states between the *ortho*-intermediate and the *meta*-intermediate ($E_0^{\mathrm{ortho}}(\mathbf{R}) - E_0^{\mathrm{meta}}(\mathbf{R})$) when the cavity polarization $\hat{e} = (\theta_1, \phi_1)$. (b) Relative energy for the *para*-intermediate and the *meta*-intermediate ($E_0^{\mathrm{para}}(\mathbf{R}) - E_0^{\mathrm{meta}}(\mathbf{R})$), for $\hat{e} = (\theta_2, \phi_2)$. These relative energies are reported as functions of the cavity mode volume $\mathcal{V}$ and cavity frequency ω_c. The color scales indicate the relative energy, with red showing thermodynamic favorability for the *meta*-substituted cation and blue for the other. The black open circles correspond to a cavity volume of $\mathcal{V} = 0.15$ nm^3 and a cavity frequency of $\omega_c = 1.8$ eV. This volume corresponds to $A_0 = 0.3$ a.u. and $\lambda = \sqrt{2\omega_c} A_0 \sim 0.1$ a.u.

nano-particle about $\omega_c \approx 2.5$ eV (500 nm) and aluminum nano-particle about $\omega_c \approx 3$ eV (400 nm).[23] In particular, for the recent experiments[48,49] on a single emitter strongly coupled to the plasmonic nano-cavity, with gold nano-particle the cavity has a frequency of $\omega_c = 1.8$ eV. Assuming mode volumes eqivalent to those previously reported (

$\mathcal{V} = 0.15$ nm^3), the equivalent coupling strength is $A_0 = 0.3$ a.u. (or $\lambda = 0.1$ a.u.) and field intensity is $\mathcal{E} = 10.9$ V/nm. With these parameters, one can lower the energy of *ortho*-complex by 6.74 kcal/mol compared to the *meta*-substituted intermediate and lower the energy of *para*-substituted intermediate by 2.24 kcal/mol compared to the *meta*-substituted intermediate. Although coupling to the cavity does not dramatically lower the energy of the *ortho/para*-substituted intermediates, these computed coupling strengths indicate favorability for the *ortho* or *para* products, and thus one should expect to obtain the mixtures of these products together with the *meta*-substituted product.

Fig. 4 presents the relative stability of the three positively charged intermediate species when cavity (a) polarized along the $\hat{\mathbf{e}} = (\theta_1, \phi_1)$ direction (primary axis of the molecule) or (b) polarized along the $\hat{\mathbf{e}} = (\theta_2, \phi_2)$ direction. The relative energy difference is reported as (a) the polaritonic ground states between the *ortho*-PhNO$_2$-Br$^+$ and the *meta*-PhNO$_2$-Br$^+$ cationic intermediate species, denoted as $E_0^{ortho}(\mathbf{R}) - E_0^{meta}(\mathbf{R})$ and (b) $E_0^{para}(\mathbf{R}) - E_0^{meta}(\mathbf{R})$. The cavity induces a stabilization of the *ortho* (*para*) species in comparison to the *meta* by up to ∼8 kcal/mol (6 kcal/mol) with cavity frequency $\omega_c = 4.0$ eV (2.5 eV) and cavity volume $\mathcal{V} = 0.1$ nm^3 (0.1 nm^3). The white region indicates the turning point of the cavity-mediated selectivity for each polarization. For the *ortho/meta* selectivity, the cavity is required to have a mode volume $\mathcal{V}$ are required to be (for $\omega_c \sim 2.5$ eV) $\mathcal{V} \sim 0.7$ nm^3 in order to favor the *ortho* selectivity. For para to be the favored product over the meta, the cavity is required to have (for $\omega_c \sim 1.5$ eV) a mode volume of $\mathcal{V} \sim 0.25$ nm^3. For reference, the volume of a single molecule (roughly the size of benzene) is ∼0.1 nm^3. In both panels, the open circles indicate currently accessible cavity parameters based on state-of-the-art NPoM plasmonic cavities[23] and correspond to a cavity volume of $\mathcal{V} = 0.15$ nm^3 and cavity frequency $\omega_c = 1.8$ eV. At these parameters, and in both polarizations, we predict that the cavity is already able to provide the selectivity of this bromination reaction away from the expected *meta* product. Thus, our theoretical predictions should be experimentally realizable with current experimental cavity designs.
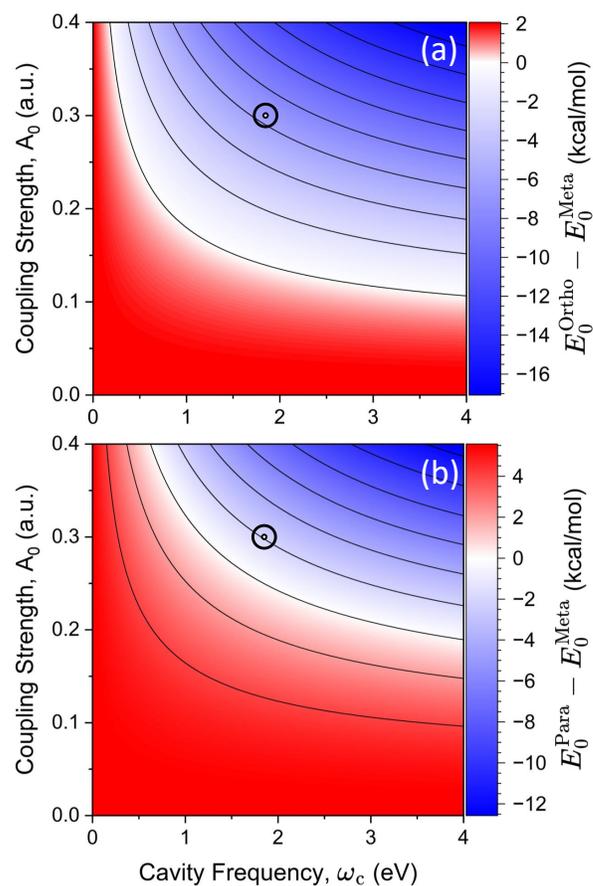
Figure 4: (a) Relative energy of the polaritonic ground states between the *ortho*-intermediate and the *meta*-intermediate ($E_0^{\mathrm{ortho}}(\mathbf{R}) - E_0^{\mathrm{meta}}(\mathbf{R})$) when the cavity polarization $\hat{\mathbf{e}} = (\theta_1, \phi_1)$. (b) Relative energy for the *para*-intermediate and the *meta*-intermediate ($E_0^{\mathrm{para}}(\mathbf{R}) - E_0^{\mathrm{meta}}(\mathbf{R})$), for $\hat{\mathbf{e}} = (\theta_2, \phi_2)$. These relative energies are reported as functions of the light-matter coupling strength A_0 and cavity frequency ω_c. The color scales indicate the relative energy, with red showing thermodynamic favorability for the *meta*-substituted cation and blue for the other. The black open circles correspond to a cavity volume of $\mathcal{V} = 0.15$ nm^3 and a cavity frequency of $\omega_c = 1.8$ eV. This volume corresponds to $A_0 = 0.3$ a.u. and $\lambda = \sqrt{2\omega_c}A_0 = 0.11$ a.u.

Conclusions.

In this work, we use the *ab initio* cavity Quantum Electrodynamics approach to investigate a chemical reaction, the bromination of nitrobenzene, coupled to an optical cavity. Our approach is based on the previously developed parametrized QED (pQED) method, which uses the QED Pauli-Fierz Hamiltonian to describe light and matter interac-

tions and uses adiabatic electronic states and all dipole matrix elements between them as inputs to compute the polariton eigenenergies.[16]

The bromination of nitrobenzene exhibits near 100% selectivity, favoring the *meta*-substituted isomer. Upon coupling to the cavity, we theoretically calculate the relative energies of the *meta*-, *ortho*-, and *para*-substituted cationic intermediates $PhNO_2$-Br^+, which are key intermediates that dictate the outcome of the reaction. Outside the cavity, the *meta*-substituted intermediate is 2 kcal/mol lower than the *ortho*-substituted intermediate and about 5 kcal/mol lower than the *para*-substituted intermediate, in agreement with reported experimental results. Upon coupling to the cavity and aligning the cavity polarization direction along the $\hat{\mathbf{e}} = (\theta_1, \phi_1)$ (see Fig. 1a), the *ortho*-substituted intermediate is energetically more stable than the *meta*-substituted intermediate by up to 6 kcal/mol for a cavity frequency ω_c and cavity volume $\mathcal{V}$ chosen to match state-of-the-art plasmonic cavity designs.[23] When the cavity polarization direction is along the $\hat{\mathbf{e}} = (\theta_2, \phi_2)$ (see Fig. 1b), the *para*-substituted intermediate is energetically more stable than the *meta*-substituted intermediate, with up to -2 kcal/mol. These changes in the selectivity of the various substituted intermediates are due to the quantum light-matter interactions between the molecules and cavity, which mixes the character of electronic excited states into the polariton ground state. These changes are characterized using the electronic density difference of the system inside and outside the cavity. We thus have theoretically shown that one can obtain *ortho*- or *para*-substituted bromonitrobenzene when coupling the reaction to an optical cavity, flipping the selectivity compared to outside the cavity.

To probe the possibility of experimental realization of our theoretical prediction, we focus on the currently available plasmonic nano-cavity parameters for the cavity frequency and field strength. We further scanned all possible polarization directions. Interestingly, we can find finite regions in the configuration space of polar angle and azimuthal angle which make the *ortho*- or *para*-substituted species more stable than the *meta*-substituted intermediate, with the largest stabilization energy of 6.43 kcal/mol (11.24 k_BT at room temperature) for *ortho* and 1.97 kcal/mol (3.42 k_BT) for *para*. The relative probability of forming the *ortho*- and *para*-substituted species is $\mathcal{P}_{ortho}/\mathcal{P}_{meta} = \exp[-(E_{ortho} - E_{meta})/k_BT] = \sim 7 \times 10^5$ for *ortho*

and $\mathcal{P}_{para}/\mathcal{P}_{meta} = 30$ for *para*. This implies that with the nano-cavity, and fully isotropic orientations of the molecule inside, one should expect to generate a non-*meta* substituted product, demonstrating that coupling to cavity can make the non-standard product which can not be easily obtained otherwise. More importantly, we have explicitly shown that coupling to a photonic cavity will will dramatically change the selectivity. Furthermore, from an experimental perspective, detection of these anomalous products will provide conclusive evidence of the cavity-mediated effects in the ground state.

From a synthetic perspective, coupling to the cavity flips the selectivity expected for electrophilic aromatic substitution in two important and useful ways. First, it flips the normal selectivity of the nitrogroup to make it an *ortho*-/*para*-director. Second, this approach appears to stabilize *ortho*-substitution over *para*-substitution. As noted above, this is also a rare selectivity that would complement existing approaches well.[52]

Overall, this work demonstrates the possibility of polariton-mediated changes to the selectivity of well-known chemical reactions. The theoretical prediction can, in principle, be experimentally verified using state-of-the-art plasmonic nano-cavity designs.

Theoretical Methods.

We use the *ab initio* polariton approach we developed in a previous work, which we refer to as the parametrized-QED (pQED) approach.[16] The pQED approach uses the Pauli-Fierz Hamiltonian in the Born-Oppenheimer approximation (see Eq. 2) to describe light and matter interactions and use adiabatic electronic states as the basis for the electronic degrees of freedom and Fock states as the basis for the photonic degree of freedom.

The light-matter interaction Hamiltonian under the dipole gauge[1,9,27] is expressed as

$$\hat{H}_{PF} = \hat{H}_{el} + \hat{H}_{ph} + \omega_c A_0 \hat{\boldsymbol{\mu}} \cdot \hat{\mathbf{e}}(\hat{a}^\dagger + \hat{a}) + \omega_c A_0^2 (\hat{\boldsymbol{\mu}} \cdot \hat{\mathbf{e}})^2, \tag{2}$$

where $\hat{H}_{el}$ is the electronic Hamiltonian under the Born-Oppenheimer approximation (*i.e.*, without the nuclear kinetic energy operator), $\hat{H}_{ph} = \omega_c \hat{a}^\dagger \hat{a}$ is the Hamiltonian of the cavity field, $\hat{a}^\dagger$ and $\hat{a}$ are the raising and lowering operators of the cavity field, $\hat{\mathbf{e}}$ is a unit vector indicating the field polarization direction, and $\hat{\boldsymbol{\mu}}$ is the dipole operator of

the molecule. Through the light-matter coupling terms in Eq. 2, various photon-dressed electronic states will be coupled to each other. For example, $|\psi_g, 1\rangle \equiv |\psi_g\rangle \otimes |1\rangle$ (the ground electronic state with 1 photon) and $|\psi_e, 0\rangle \equiv |\psi_e\rangle \otimes |0\rangle$ (an excited electronic state with 0 photons) will couple through $\langle\psi_g, 1|\hat{\boldsymbol{\mu}} \cdot \hat{\mathbf{e}}(\hat{a}^\dagger + \hat{a})|e, 0\rangle = \mu_{ge}\langle 1|(\hat{a}^\dagger + \hat{a})|0\rangle$, where μ_{ge} is the transition dipole between the ground state and excited state projected along the $\hat{\mathbf{e}}$ direction. When the energy of these two basis states become close, the $|\psi_g, 1\rangle$ and $|\psi_e, 0\rangle$ states hybridize, leading to the formation of excited polariton states. This is the typical resonant light-matter coupling induced hybridization and generating new eigenstates, and polaritons.

Direct modification of polariton ground states, can be caused by two other physical processes:[1,9,29] (i) off-resonance light-matter interactions (third term in Eq. 2) through the ground state permanent dipole and optical transition dipoles between the ground and excited states, and (ii) a dipole self-energy (DSE) term (final term in Eq. 2). For example, in (i), $|\psi_g, 0\rangle$ will couple to $|\psi_g, 1\rangle$ state through a term proportional to $\langle\psi_g, 0|\hat{\mu}(\hat{a}^\dagger + \hat{a})|\psi_g, 1\rangle = \mu_{gg}\langle 0|(\hat{a}^\dagger + \hat{a})|1\rangle = \mu_{gg}$, and $|\psi_g, 1\rangle$ will couple to $|\psi_e, 0\rangle$ through $\langle\psi_e, 0|\hat{\mu}(\hat{a}^\dagger + \hat{a})|\psi_g, 1\rangle = \mu_{ge}\langle 0|(\hat{a}^\dagger + \hat{a})|1\rangle = \mu_{ge}$. Note that there may be many such electronic excited states ψ_e that contribute to the ground state through these off-resonant interactions (See **Supporting Information** for details on specific interaction terms depicted through an analysis of the ground state density matrix). In (ii), the DSE term allows for extensive coupling through the square of the electronic dipole matrix $(\hat{\boldsymbol{\mu}} \cdot \hat{\mathbf{e}})^2 \equiv \hat{\mu}^2$ where we denote $\hat{\mu}$ as the projection of $\hat{\boldsymbol{\mu}}$ along the cavity polarization direction $\hat{\mathbf{e}}$. The matrix elements between the ground state $|\psi_g\rangle$ and any electronic state $|\psi_\alpha\rangle$ due to the DSE coupling can be expressed as $\langle\psi_g|\hat{\mu}^2|\psi_\alpha\rangle = \sum_\gamma \mu_{g\gamma}\mu_{\gamma\alpha}$, where α and γ include the ground and excited electronic states. The direct coupling (i) is responsible for the accumulation of photons in the ground state[10] while DSE (ii) is largely responsible for the modifications to the ground state energy.[53]

The polariton eigenstates and eigenenergies are obtained by solving the following equation

$$\hat{H}_{\mathrm{PF}}|\Phi_j(\mathbf{R})\rangle = E_j(\mathbf{R})|\Phi_j(\mathbf{R})\rangle, \qquad (3)$$

where $\hat{H}_{\mathrm{PF}}$ is given in Eq. 2, $E_j(\mathbf{R})$ is the Born-Oppenheimer polaritonic potential energy surfaces (which parametrically depend on the nuclear coordinates $\mathbf{R}$), and $|E_j(\mathbf{R})\rangle$ is the polariton state. We directly diagonalize the polaritonic Hamiltonian $\hat{H}_{\mathrm{PF}}$ matrix and obtain the eigenvalues. The basis is constructed using the tensor product of electronic adiabatic states $|\psi_\alpha(\mathbf{R})\rangle$ (*i.e.*, eigenstates of the electronic Hamiltonian $\hat{H}_{\mathrm{el}}$) and the Fock states $|n\rangle$ (*i.e.*, eigenstates of the photonic Hamiltonian $\hat{H}_{\mathrm{ph}}$), expressed as $|\psi_\alpha(\mathbf{R})\rangle \otimes |n\rangle \equiv |\psi_\alpha(\mathbf{R}), n\rangle$. This basis is used to evaluate the matrix elements of $\hat{H}_{\mathrm{PF}}$, and diagonalizing it provides $E_j(\mathbf{R})$ and the corresponding polariton states

$$|\Phi_j(\mathbf{R})\rangle = \sum_\alpha^{\mathcal{N}_{\mathrm{el}}} \sum_n^{\mathcal{N}_{\mathrm{F}}} C_{\alpha n}^j |\psi_\alpha(\mathbf{R}), n\rangle, \qquad (4)$$

where $C_{\alpha n}^j = \langle\psi_\alpha(\mathbf{R}), n|\Phi_j(\mathbf{R})\rangle$. Here, the number of included electronic states, $\mathcal{N}_{\mathrm{el}}$, and photonic Fock/number states, $\mathcal{N}_{\mathrm{F}}$, are treated as convergence parameters. A convergence test is provided in the **Supporting Information**, and the typical numbers of states are $\mathcal{N}_{\mathrm{F}} = 5$ and $\mathcal{N}_{\mathrm{el}} = 50$. Further details regarding the pQED approach are provided in the **Supporting Information**. The accuracy of the above-described pQED approach has been benchmarked[16] with the more accurate self-consistent QED coupled-cluster (scQED-CC) approach, where the pQED method generates nearly quantitative agreement with the scQED-CC approach.

All electronic structure calculations were performed using the QCHEM software package[54] using linear response time-dependent density functional theory (LR-TD-DFT) and the ωB97XD hybrid exchange-correlation functional with the 6-311+G* basis set. The geometries of the PhNO$_2$-Br$^+$ intermediate with various substitution positions are optimized in its electronic ground states. For cavity polarization $\hat{\mathbf{e}}$ along a particular direction with (θ, ϕ) angles, the $\hat{\boldsymbol{\mu}} \cdot \hat{\mathbf{e}}$ term in Eq. 2 is evaluated as follows

$$\hat{\boldsymbol{\mu}} \cdot \hat{\mathbf{e}} = \sin\theta\cos\phi\, \hat{\boldsymbol{\mu}} \cdot \mathbf{X} + \sin\theta\sin\phi\, \hat{\boldsymbol{\mu}} \cdot \mathbf{Y} + \cos\theta\, \hat{\boldsymbol{\mu}} \cdot \mathbf{Z}, \qquad (5)$$

where $\hat{\boldsymbol{\mu}} \cdot \mathbf{X}$, $\hat{\boldsymbol{\mu}} \cdot \mathbf{Y}$, $\hat{\boldsymbol{\mu}} \cdot \mathbf{Z}$ are the dipole operator projected along $\mathbf{X}$, $\mathbf{Y}$, and $\mathbf{Z}$ directions. The matrix elements of these projected dipole operators, $\langle\psi_\alpha|\hat{\boldsymbol{\mu}} \cdot \mathbf{X}|\psi_\gamma\rangle$, $\langle\psi_\alpha|\hat{\boldsymbol{\mu}} \cdot \mathbf{Y}|\psi_\gamma\rangle$, and $\langle\psi_\alpha|\hat{\boldsymbol{\mu}} \cdot \mathbf{Z}|\psi_\gamma\rangle$ are obtained from electronic structure calculations and are used to evaluate the $\hat{\mathbf{e}} \cdot \hat{\boldsymbol{\mu}}$ term in Eq. 2. The electronic excited state energies and the molecular transition dipole matrix were computed using the

QCHEM package.[54]

Supporting Information Available

Details of Theoretical Approaches; Theoretical Analysis of the Energy Contributions for Polariton Ground State; Additional Results on Density Difference; Convergence of the Calculation with Adiabatic-Fock Basis; Additional Analysis of the Ground State Density Matrix.

References

(1) Mandal, A.; Taylor, M. A. D.; Weight, B. M.; Koessler, E. R.; Li, X.; Huo, P. Theoretical Advances in Polariton Chemistry and Molecular Cavity Quantum Electrodynamics. **2023**, *123*, 9786–9879.

(2) Zeng, H.; Pérez-Sánchez, J. B.; Eckdahl, C. T.; Liu, P.; Chang, W. J.; Weiss, E. A.; Kalow, J. A.; Yuen-Zhou, J.; Stern, N. P. Control of Photoswitching Kinetics with Strong Light–Matter Coupling in a Cavity. *J. Am. Chem. Soc.* **2023**,

(3) Hutchison, J. A.; Schwartz, T.; Genet, C.; Devaux, E.; Ebbesen, T. W. Modifying Chemical Landscapes by Coupling to Vacuum Fields. *Angew. Chem. Int. Ed.* **2012**, *51*, 1592–1596.

(4) Lather, J.; Bhatt, P.; Thomas, A.; Ebbesen, T. W.; George, J. Cavity Catalysis by Cooperative Vibrational Strong Coupling of Reactant and Solvent Molecules. *Angew. Chem. Int. Ed.* **2019**, *58*, 10635–10638.

(5) Lather, J.; Thabassum, A. N. K.; Singh, J.; George, J. Cavity catalysis: modifying linear free-energy relationship under cooperative vibrational strong coupling. *Chem. Sci.* **2022**, *13*, 195–202.

(6) Thomas, A.; George, J.; Shalabney, A.; Dryzhakov, M.; Varma, S. J.; Moran, J.; Chervy, T.; Zhong, X.; Devaux, E.; Genet, C.; Hutchison, J. A.; Ebbesen, T. W. Ground-State Chemical Reactivity under Vibrational Coupling to the Vacuum Electromagnetic Field. *Angew. Chem. Int. Ed.* **2016**, *55*, 11462–11466.

(7) Thomas, A.; Jayachandran, A.; Lethuillier-Karl, L.; Vergauwe, R. M. A.; Nagarajan, K.; Devaux, E.; Genet, C.; Moran, J.; Ebbesen, T. W. Ground state chemistry under vibrational strong coupling: dependence of thermodynamic parameters on the Rabi splitting energy. *Nanophotonics* **2020**, *9*, 249–255.

(8) Thomas, A.; Lethuillier-Karl, L.; Nagarajan, K.; Vergauwe, R. M. A.; George, J.; Chervy, T.; Shalabney, A.; Devaux, E.; Genet, C.; Moran, J.; Ebbesen, T. W. Tilting a ground-state reactivity landscape by vibrational strong coupling. *Science* **2019**, *363*, 615–619.

(9) Mandal, A.; Taylor, M. A. D.; Huo, P. Theory for Cavity-Modified Ground-State Reactivities via Electron–Photon Interactions. *J. Phys. Chem. A* **2023**, *127*, 6830–6841.

(10) Flick, J.; Schäfer, C.; Ruggenthaler, M.; Appel, H.; Rubio, A. Ab Initio Optimized Effective Potentials for Real Molecules in Optical Cavities: Photon Contributions to the Molecular Ground State. *ACS Photonics* **2018**, *5*, 992–1005.

(11) Haugland, T. S.; Ronca, E.; Kjønstad, E. F.; Rubio, A.; Koch, H. Coupled Cluster Theory for Molecular Polaritons: Changing Ground and Excited States. *Phys. Rev. X* **2020**, *10*, 041043.

(12) Mordovina, U.; Bungey, C.; Appel, H.; Knowles, P. J.; Rubio, A.; Manby, F. R. Polaritonic coupled-cluster theory. *Phys. Rev. Research* **2020**, *2*, 023262.

(13) DePrince, A. E. Cavity-modulated ionization potentials and electron affinities from quantum electrodynamics coupled-cluster theory. *J. Chem. Phys.* **2022**, *154*, 094112.

(14) Riso, R. R.; Haugland, T. S.; Ronca, E.; Koch, H. Molecular orbital theory in cavity QED environments. *Nat. Commun.* **2022**, *13*, 1368.

(15) Pavošević, F.; Hammes-Schiffer, S.; Rubio, A.; Flick, J. Cavity-Modulated Proton Transfer Reactions. *J. Am. Chem. Soc.* **2022**, *144*, 4995–5002.

(16) Weight, B. M.; Krauss, T. D.; Huo, P. Investigating Molecular Exciton Polaritons Using Ab Initio Cavity Quantum Electrodynamics. *J. Phys. Chem. Lett.* **2023**, *14*, 5901–5913.

(17) Weight, B. M.; Tretiak, S.; Zhang, Y. Diffusion quantum Monte Carlo approach to the polaritonic ground state. *Phys. Rev. A* **2024**, *109*, 032804.

(18) Severi, M.; Zerbetto, F. Polaritonic Chemistry: Hindering and Easing Ground State Polyenic Isomerization via Breakdown of $\sigma-\pi$ Separation. *J. Phys. Chem. Lett.* **2023**, *TBA*, 9145–9149.

(19) Weight, B. M.; Li, X.; Zhang, Y. Theory and modeling of light-matter interactions in chemistry: current and future. *Phys. Chem. Chem. Phys.* **2023**,

(20) Pavošević, F.; Smith, R. L.; Rubio, A. Computational study on the catalytic control of endo/exo Diels-Alder reactions by cavity quantum vacuum fluctuations. *Nat Commun* **2023**, *14*, 2766.

(21) Wang, J.; Weight, B.; Huo, P. Investigating Cavity Quantum Electrodynamics-Enabled Endo/Exo- Selectivities in a Diels-Alder Reaction. **2024**,

(22) Pavosevic, F.; Smith, R. L.; Rubio, A. Cavity Click Chemistry: Cavity-Catalyzed Azide-Alkyne Cycloaddition. *J. Phys. Chem. A.* **2023**, *127*, 10184–10188.

(23) Akselrod, G. M.; Huang, J.; Hoang, T. B.; Bowen, P. T.; Su, L.; Smith, D. R.; Mikkelsen, M. H. Large-Area Metasurface Perfect Absorbers from Visible to Near-Infrared. *Advanced Materials* **2015**, *27*, 8028–8034.

(24) Vu, N.; Mejia-Rodriguez, D.; Bauman, N.; Panyala, A.; Mutlu, E.; Govind, N.; Foley, J. Cavity Quantum Electrodynamics Complete Active Space Configuration Interaction Theory. *J. Chem. Theory Comput.* **2024**, *20*, 1214–1227.

(25) Li, X.; Zhang, Y. First-principles molecular quantum electrodynamics theory at all coupling strengths. **2023**, arXiv:2310.18228 [physics].

(26) Cui, Z.-H.; Mandal, A.; Reichman, D. R. Variational Lang–Firsov Approach Plus Møller–Plesset Perturbation Theory with Applications to Ab Initio Polariton Chemistry. *J. Chem. Theory Comput.* **2024**, *20*, 1143–1156.

(27) Taylor, M. A. D.; Mandal, A.; Zhou, W.; Huo, P. Resolution of Gauge Ambiguities in Molecular Cavity Quantum Electrodynamics. *Phys. Rev. Lett.* **2020**, *125*, 123602.

(28) Jaynes, E. T.; Cummings, F. W. Comparison of quantum and semiclassical radiation theories with application to the beam maser. *Proc. IEEE* **1963**, *51*, 89–109.

(29) Mandal, A.; Vega, S. M.; Huo, P. Polarized Fock States and the Dynamical Casimir Effect in Molecular Cavity Quantum Electrodynamics. *J. Phys. Chem. Lett.* **2020**, *11*, 9215–9223.

(30) Loudon, M.; Parise, J. *Organic Chemistry*; Macmillan Learning, 2015.

(31) Anslyn, E. V.; Dougherty, D. A. *Modern Physical Organic Chemistry*; University Science Books, 2006.

(32) Harrison, J. J.; Pellegrini, J. P.; Selwitz, C. M. Bromination of deactivated aromatics using potassium bromate. *J. Org. Chem.* **1981**, *46*, 2169–2171.

(33) Rozen, S.; Brand, M.; Lidor, R. Aromatic bromination using bromine fluoride with no Friedel-Crafts catalyst. *J. Org. Chem.* **1988**, *53*, 5545–5547.

(34) Tanemura, K.; Suzuki, T.; Nishida, Y.; Satsumabayashi, K.; Horaguchi, T. Halogenation of Aromatic Compounds by N-chloro-, N-bromo-, and N-iodosuccinimide. *Chemistry Letters* **2003**, *32*, 932–933.

(35) Eguchi, H.; Kawaguchi, H.; Yoshinaga, S.; Nishida, A.; Nishiguchi, T.; Fujisaki, S. Halogenation Using N-Halogenocompounds. II. Acid Catalyzed Bromination of Aromatic Compounds with 1,3-Dibromo-5,5-dimethylhydantoin. *Bulletin of the Chemical Society of Japan* **1994**, *67*, 1918–1921.

(36) Wang, W.; Yang, X.; Dai, R.; Yan, Z.; Wei, J.; Dou, X.; Qiu, X.; Zhang, H.; Wang, C.; Liu, Y.; Song, S.; Jiao, N. Catalytic Electrophilic Halogenation of Arenes with Electron-Withdrawing Substituents. *J. Am. Chem. Soc.* **2022**, *144*, 13415–13425.

(37) Almeida, L. S. d.; Mattos, M. C. S. d.; Esteves, P. M. Tribromoisocyanuric Acid in Trifluoroacetic Acid: An Efficient System for Smooth Brominating of Moderately Deactivated Arenes. *Synlett* **2013**, *24*, 603–606.

(38) Chattaraj, P. K., Ed. *Chemical Reactivity Theory: A Density Functional View*; CRC Press: Boca Raton, 2009.

(39) Arrieta, A.; Cossı́o, F. P. Loss of aromaticity and -electron delocalization in the first step of the electrophilic aromatic nitration of benzene, phenol and benzonitrile. *Journal of Molecular Structure: THEOCHEM* **2007**, *811*, 19–26.

(40) Deraet, X.; Desmedt, E.; Lommel, R. V.; Speybroeck, V. V.; Proft, F. D. The electrophilic aromatic bromination of benzenes: mechanistic and regioselective insights from density functional theory. *Phys. Chem. Chem. Phys.* **2023**, *25*, 28581–28594.

(41) Rohrbach, S.; Murphy, J. A.; Tuttle, T. Computational Study on the Boundary Between the Concerted and Stepwise Mechanism of Bimolecular SNAr Reactions. *J. Am. Chem. Soc.* **2020**, *142*, 14871–14876.

(42) Moors, S. L. C.; Deraet, X.; Assche, G. V.; Geerlings, P.; Proft, F. D. Aromatic sulfonation with sulfur trioxide: mechanism and kinetic model. *Chem. Sci.* **2016**, *8*, 680–688.

(43) Van Lommel, R.; Moors, S. L. C.; De Proft, F. Solvent and Autocatalytic Effects on the Stabilisation of the σ-Complex during Electrophilic Aromatic Chlorination. *Chemistry – A European Journal* **2018**, *24*, 7044–7050.

(44) Stuyver, T.; Danovich, D.; De Proft, F.; Shaik, S. Electrophilic Aromatic Substitution Reactions: Mechanistic Landscape, Electrostatic and Electric-Field Control of Reaction Rates, and Mechanistic Crossovers. *J. Am. Chem. Soc.* **2019**, *141*, 9719–9730.

(45) Makhloufi, A.; Belhadad, O.; Ghemit, R.; Baitiche, M.; Merbah, M.; Benachour, D. Theoretical and conceptual density functional theory (DFT) study on selectivity of 4-hydroxyquinazoline electrophilic aromatic nitration. *Journal of Molecular Structure* **2018**, *1152*, 248–256.

(46) Kong, J.; Galabov, B.; Koleva, G.; Zou, J.-J.; Schaefer III, H. F.; Schleyer, P. v. R. The Inherent Competition between Addition and Substitution Reactions of Br2 with Benzene and Arenes. *Angewandte Chemie International Edition* **2011**, *50*, 6809–6813.

(47) Galabov, B.; Koleva, G.; Simova, S.; Hadjieva, B.; Schaefer, H. F.; Schleyer, P. v. R. Arenium ions are not obligatory intermediates in electrophilic aromatic substitution. *Proceedings of the National Academy of Sciences* **2014**, *111*, 10067–10072.

(48) Chikkaraddy, R.; de Nijs, B.; Benz, F.; Barrow, S. J.; Scherman, O. A.; Rosta, E.; Demetriadou, A.; Fox, P.; Hess, O.; Baumberg, J. J. Single-molecule strong coupling at room temperature in plasmonic nanocavities. *Nature* **2016**, *535*, 127–130.

(49) Santhosh, K.; Bitton, O.; Chuntonov, L.; Haran, G. Vacuum Rabi splitting in a plasmonic cavity at the single quantum emitter limit. *Nat. Commun.* **2016**, *7*, 1–5.

(50) Wu, T.; Yan, W.; Lalanne, P. Bright Plasmons with Cubic Nanometer Mode Volumes through Mode Hybridization. *ACS Photonics* **2021**, *8*, 307–314.

(51) Chen, S.; Xiao, Y.-H.; Qin, M.; Zhou, G.; Dong, R.; Devasenathipathy, R.; Wu, D.-Y.;

12

Yang, L. Quantification of the Real Plasmonic Field Transverse Distribution in a Nanocavity Using the Vibrational Stark Effect. *J. Phys. Chem. Lett.* **2023**, *14*, 1708–1713.

(52) Srivastava, S. K.; Chauhan, P. M. S.; Bhaduri, A. P. Novel site-specific one-step bromination of substituted benzenes. *Chem. Commun.* **1996**, 2679–2680.

(53) Rokaj, V.; Welakuh, D. M.; Ruggenthaler, M.; Rubio, A. Light–matter interaction in the long-wavelength limit: no ground-state without dipole self-energy. *J. Phys. B: At. Mol. Opt. Phys.* **2018**, *51*, 034005.

(54) Epifanovsky, E. et al. Software for the frontiers of quantum chemistry: An overview of developments in the Q-Chem 5 package. *J. Chem. Phys.* **2021**, *155*, 084801.

13

TOC Graphic